Specimen designs for accurate tensile testing of unidirectional composite laminates

Babak Fazlali[1], Shailee Upadhyay[1], Sagar Ashokbhai Ashodia[1,2], Francisco Mesquita[1], Stepan V. Lomov[1], Valter Carvelli[2], Yentl Swolfs[1]

[1] Department of Materials Engineering, KU Leuven, Kasteelpark Arenberg 44 bus 2450, Belgium.
[2] Department of Architecture, Built Environment and Construction Engineering, Politecnico di Milano, Piazza Leonardo Da Vinci 32, 20133, Milan, Italy.

Abstract

Tensile testing of unidirectional composites based on standardized test methods nearly always leads to premature failure in the end tab region. The material near the tab section is under a complex loading state, including longitudinal, transverse, and shear stress components. The present work examines different conventional designs for tensile testing along with novel ones to find the method that minimizes the geometric discontinuity and yields the highest failure strain. Finite element (FE) models are utilized to predict the stress concentrations for all end tab designs with representation of the actual grip components. The simulation reveals that the stress concentration near the edge of the end tabs can vary significantly with end tab design. FE models are used to further optimize the geometry of end tabs. The experimental results reveal that specimens with novel arrow-shaped tabs and continuous tabs yield the highest failure strain, and hence are best at avoiding premature failure.

1 Introduction

Tensile testing is the basic characterization method to define the material properties of composites. However, the ASTM and ISO standard test methods for unidirectional (UD) composites mostly lead to unacceptable failure near the gripped section [1]. The multiaxial stress concentrations near the end tabs and the highly anisotropic behavior of UD composites triggers premature failure. This underestimates the real tensile strength and hence leads to over-dimensioned designs.

ASTM D3039/D3039M [2] and ISO 527-1 [3] are commonly used standards for tensile tests on high-strength UD composites. Both standards recommend rectangular (prismatic) specimen with cross-ply E-glass/epoxy with the fibers at 45° as end tabs. Tapering the end tabs at 7° along the specimen length direction instead of a straight cut is suggested to have a gradual reduction of cross-section and consequently decrease stress concentrations. However, even these recommendations often do not lead to failure inside the gauge section and away from end tabs [4–6].

In the literature, there are few studies on modifying tensile specimen design that leads to gauge section failure of UD composites. Hojo et al. [7] performed a round-robin test to investigate the effect of tab design and gripping conditions on the tensile properties of carbon/epoxy UD composites. There was no considerable difference in tensile strength for specimens with rectangular and tapered end tabs. Kulakov et al. [8], however, reported a 10% increase in failure strain for tapered end tabs with an angle less than

10° compared to straight end tabs. The tapered end tabs reduce the stress concentration by reducing the geometric discontinuity. However, the lack of gripping pressure on the tapered section caused delamination between end tabs and specimen which could lead to premature failure [9]. Silva et al. [10] proposed some geometries for the forward edge of the end tab to reduce the normal (through the thickness) stress and delay or suppress the delamination. Khan et al. [11] proposed tapering specimens by using ply drops to suppress the delamination. This type of tapering enabled gauge section failure and increased the obtained strength by 14.5%. Kulakov et al. [8] further presented a parametric study of specimen geometry, end tab material and geometry and adhesive material to calculate the multiaxial stress concentrations near the end tabs. They simulated the actual set-up of the tensile grips to define the stress and strain along the specimen length during loading. They concluded that a tapered glass fiber composite end tab bonded by a low-modulus adhesive could result in gauge section failure.

Portnov et al. [12,13] carried out finite element (FE) analysis by simulating the actual set-up of the tensile grips and considering the elastoplastic behavior of the adhesive. They investigated the effect of end tab geometry and grip misalignment on stress concentrations near the end tabs. They emphasized the effect of modeling the elastoplastic behavior of adhesive on stress concentration underneath the gripped section. Their parametric study revealed a 3.3-fold increase in maximum normal stress in the gripped section after changing the position of wedge grips (from the end tab completely inside to partially outside of the grip) and 3.7-fold with a change in end tab geometry. They also studied the effect of grip misalignment on stress concentration. Just 1 mm of misalignment in the normal direction over a gauge length of 200 mm caused 2% extra longitudinal stress concentration at the forward edge of the end tab.

All the mentioned studies tried to minimize the stress concentrations near the tabbed section but could not eliminate them. Czél et al. [14] proposed continuous UD S-glass tabs to protect the specimen from stress concentrations in gripped section. They exploited a 2D FE model and proved that the stress concentration in specimens with continuous tabs is suppressed. This tab also protects the specimen from surface damage. They reported that the specimen with continuous tabs failed at about 22% higher strain compared to the specimen with rectangular end tabs.

Another promising approach to obtain failure in the gauge section is a butterfly or dog-bone shaped specimen [15–17]. Butterfly or dog-bone shaped specimens remove stress concentrations from the gauge section, which is the straight part in the middle of the specimen (see Fig. 1). The stress concentrations remain near the edge of the end tab which are far away from the gauge section area; however, the shape of the specimen may cause longitudinal splitting in the curved section. To minimize or delay the initiation of splitting, a long-butterfly (X-butterfly) specimen was introduced by Kumar et al [18] by increasing the length of the specimen and reducing the curvature. This study considered the effect of butterfly specimen on the failure strain of carbon/vinylester composites. They tested butterfly specimens with continuous tabs to eliminate the effect of the tabbed section. They reported increases of more than 11% and 17% in failure strain for long-butterfly specimens with continuous tabs compared to rectangular specimens with continuous and conventional tabs, respectively. Note that the preparation of butterfly specimens is not straightforward and needs special effort. The end tab with a thickness of 2-4 mm should be tapered down to 0 mm over a 50 mm length. The specimen with end tabs should be waterjet cut or milled to a butterfly shape.

Standard methods for UD tensile test mostly lead to unacceptable failure near the grip. Improved specimen designs yielded varying degrees of success, and all designs come with risks or drawbacks. The present work studies different end tabs and specimen designs to establish an accurate method for tensile testing of UD composites. We will examine different strategies suggested in the literature to minimize or avoid failure near end tabs, and we will introduce arrow-shape end tabs for the first time. To deeply understand the source of stress concentration, the actual set-up of tensile testing including all machine components such as wedge grip and the plunger was simulated. The same model was used to further optimize a novel arrow-shape end tab design.

2 Materials and methods

2.1 Materials

The specimens in this study were made from UD thin ply carbon fiber/epoxy HS40/736LT prepreg (North Thin Ply Technology, Switzerland). The specimens were manufactured in an autoclave with a stacking sequence of $[0]_{10}$. The cured thickness of the laminate used in all specimens was on average 0.5 mm. The end tab material consisted of woven fabric E-glass/epoxy while the continuous tabs were made from 0^{o} UD S-glass/913 epoxy (SCG75, Hexcel). The continuous tabs were cured together with the specimen. Although they have different resin systems, the proposed curing cycle of both materials was compatible. Table 1 summarizes the material properties of the specimen and tabs. The longitudinal stiffness of the HS40/epoxy UD laminate was obtained in the experimental part of the study. Note that a high-stiffness carbon fiber was used in this study. The stiffness discrepancy between the specimen and end tab intensifies the stress concentration, making it easier to measure difference between the considered specimen designs.

2.2 Tensile tests

We prepared six different designs consisting of different end tabs and specimen shape. Fig. 1 presents the geometry and dimension of each specimen. Compared to the proposed butterfly specimen in [18], the length of the gripped and tapered section was reduced from 70 mm to 50 mm due to wedge grip and manufacturing limitations. Note that we also added rectangular end tabs on the continuous tab specimen as in [14] to minimize any possible effect of wedge grip surface and yield maximum failure strain. The tensile tests were performed on a Zwick tensile machine with a load cell of 100 kN and hydraulic grips at a displacement rate of 1 mm/min. The hydraulic gripping force was adjusted to be as low as possible while avoiding slipping during the test. Preliminary tests were performed to minimize the hydraulic gripping force while avoiding sliding for each design. We therefore used 42.5 kN for continuous tab, 14 kN for butterfly, and 25.5 kN for other designs. Since the arrow-shape end tab is placed partially outside of the grip (the arrow section is out of the grip, see Fig. 1), the gripped surface area is smaller than the rectangular end tabs. The arrow-shape end tab design therefore may need a slightly higher gripping force, which can potentially lead to higher stress concentrations. Digital image correlation (VIC-2D software) was used to measure the average surface strain. A digital camera (with a lens Schneider Kreuznach componon-S 2.8/50) was used to capture the full gauge length (between end tabs for all designs except butterfly design) speckle pattern of the specimen apart from the area close to the end tabs. The averaging in VIC-2D software was performed on the full speckled region. Pictures were taken every 0.5 seconds and synchronized with the load cell signal from the tensile machine.

Table 1. Properties of UD carbon/epoxy and S/E-glass/epoxy.

Material	UD HS40/epoxy*	UD S-glass/913 epoxy	E-glass/epoxy**
Layup	$[0]_{10}$	$[0]_4$	0/90 woven
Thickness (mm)	0.5 (±0.02)	0.6	2
Nominal volume fraction (%)	56	50	50
E_{11} (GPa)	250.5 (±19)	45.7 (±3.2) [14]	28.2
E_{22} (GPa)	4.9	5.6	28.2
E_{33} (GPa)	4.9	5.6	10.3
$v_{12} = v_{13}$	0.34	0.27	0.27
v_{23}	0.30	0.27	0.27
$G_{12} = G_{13}$ (GPa)	2.6	3.2	3.1
G_{23} (GPa)	1.9	2.1	3.1
Fiber elastic modulus (GPa)	425 [19]	88 [14]	
Fiber strength (GPa)	4.61 [19]	-	-
Fiber failure strain (%)	1.1 [19]	-	-
Fiber areal density (g/m^2)	50	190 [14]	-
Fiber diameter (µm)	4.96 [19]	-	-

*Measured thickness and longitudinal elastic modulus (E_{11}) (± means standard deviation)
The rest of the properties were estimated using Chamis' [20] formulae and manufacturer's datasheet
**The number of plies is unknown

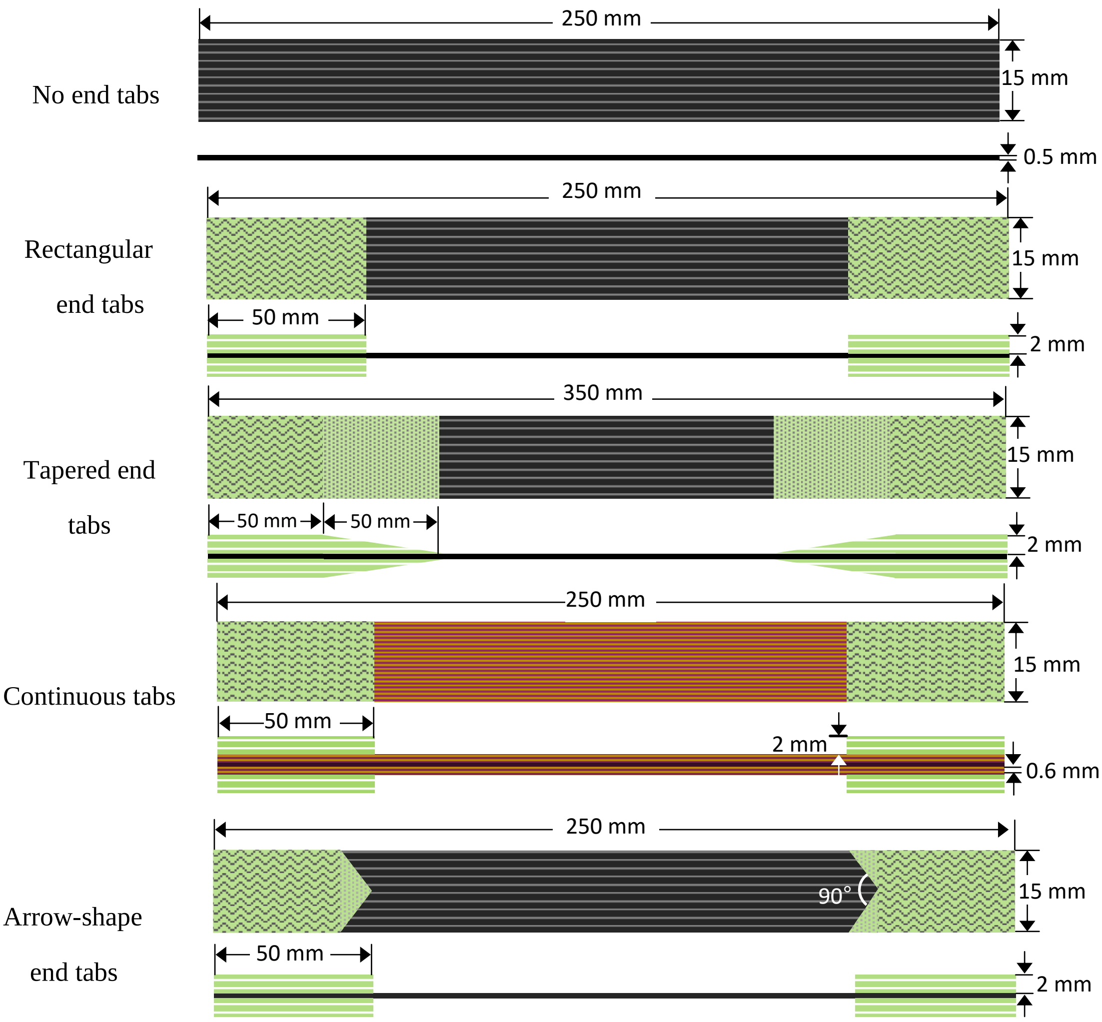

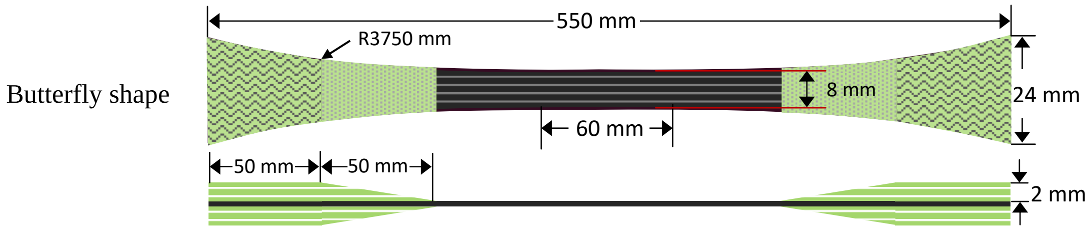

Fig. 1 *Geometry and dimension of specimens. The drawings are correctly scaled within a specimen, but not between specimens. The average thickness of all specimens is 0.5 mm and the wavy pattern on the end tabs indicates the gripped section.*

2.3 Finite element simulations

The simulation study was performed for all designs specified in Fig. 1. Table 1 summarizes the properties of the simulated materials, where notations 1 (=X), 2 (=Y), and 3 (=Z) correspond to longitudinal (0°), transverse (90°), and normal (through the thickness) directions, respectively.

FE simulations were performed using ABAQUS/CAE 2019 software. All materials were modeled as 3-dimensional, transversely isotropic, linearly elastic, homogenous solids. The simulations did not consider the damage of the materials and the non-linear stress response of the UD CF/EP composite. In several studies, a simplified tensile test setup was simulated which did not consider the machine components (see e.g. [21]). Fig. 2a presents the boundary conditions of such a simplified model. While this model provides preliminary information regarding stress distribution in the specimen, it does not account for the effect of friction between the grip components. To understand the sources of stress concentration and optimize the test setup, it is crucial to simulate the actual test setup. The present study, therefore, utilizes a test setup introduced by Portnov et al. [12] and later improved by De Baere et al. [6], which includes grip components. In this setup, three machine components were included: plunger, cylinder, and a wedge grip (see Fig. 2b).

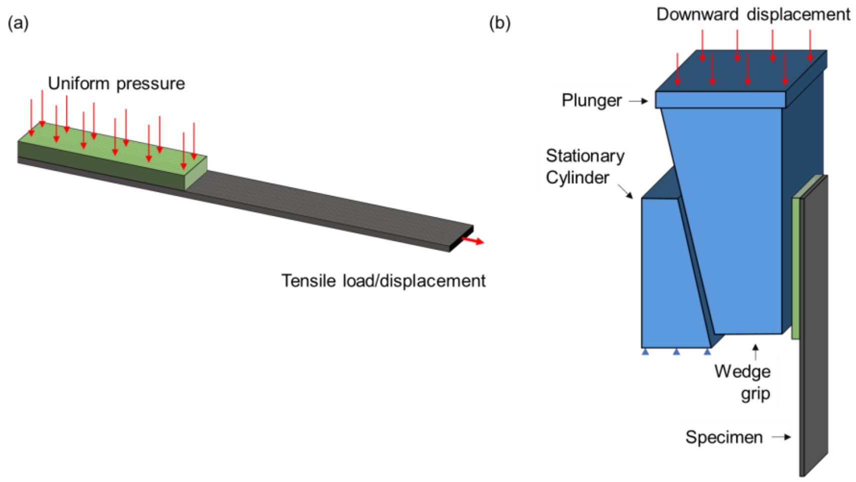

Fig. 2 *Model description: (a) boundary conditions for simplified tensile test model, and (b) representation of tensile test setup studied by De Baere et al. [6].*

The plunger and cylinder interact with the wedge grip by 'locking' the specimen. This motion provides the contact pressure for gripping the specimen. The wedge grip-specimen interface characteristic plays a key role in the stress distribution on the specimen. In the reference model by De Baere et al. [6], it was assumed that there is no slippage between grip and specimen due to grip serrations, and the interface was given a ‘rough’ contact property. In practice, however, a perfectly rough interface between specimen and wedge grip is not realistic even with serrations and slight slipping is often observed. Therefore, the present model assumes a high friction value of 0.8 between the wedge grip and the specimen instead of a ‘rough’ contact. This value was chosen based on some examples of friction contact between metal and glass or epoxy. A sensitivity analysis was performed for friction coefficients 0.7, 0.8 and 0.9, which confirmed that this parameter does not significantly influence the stress distribution.

For machine components, a low friction coefficient value of 0.16 was adopted based on the recommendation for steel-to-steel lubricated contact in [22]. A sensitivity analysis on friction conditions (frictionless, 0.1 and 0.16) reveals that the friction between components only influences the stress distribution on the machine components and has a negligible effect on the stress distribution in the specimen. The wedge grip surfaces were assigned as a slave for all friction contacts as they initially follow the movement of plunger, and then the movement of the specimen. This allows for a realistic simulation of actual testing conditions where the wedge grip follows the movement of the machine head for gripping and then the specimen during the tensile test. The model size was reduced by utilizing the symmetries along length, width, and thickness directions, in all designs except arrow-shape. In the case of arrow-shape specimen, a length symmetry does not exist and therefore only width and thickness direction symmetries were applied.

The study of Kulakov et al. [8] indicated that the introduction of epoxy adhesive does not significantly affect the longitudinal stress concentrations: only a slight softening of the longitudinal stress concentrations by about 2% was reported. We also investigated the effect of the adhesive in this study, excluding the assembly components. When adding a linearly elastic adhesive layer with an elastic modulus of 3 GPa [8] and thicknesses of 50 μm and 100 μm, a reduction in longitudinal stress concentration of 10% and 15% is observed, respectively. These results show the significant influence of adhesive thickness, demanding precise measurement of it. A few specimens were therefore cut from the middle of the end tabs to measure the adhesive thickness. The variation in the adhesive thickness makes it hard to define a specific value. Therefore, the definition of adhesive thickness and then accurate stress distribution in the tab section is challenging. As the primary objective of this study is to compare stress concentrations across different specimen designs, rather than establishing the exact value of stress concentration, it is assumed that a perfect bond exists between the specimen and end tabs.

Linear hexahedral brick elements C3D8, fully integrated (2x2x2 integration points), are used to mesh the model. A denser mesh of element size 0.01 mm was used close to the edge of the end tabs (see Fig. 3c). To optimize the computational time, the mesh was gradually increased away from the edge of the end tabs (see Fig. 3c). Since the value of stress in FE analysis can be affected by mesh size, the entire area close to end tab edges was meshed with the same size in all the designs. To achieve this in arrow-shape specimen, partitions were created in the geometry. The machine components were given a non-variable mesh. Fig. 3 presents the meshed model assembly as well as the variable mesh with a small element size under the end tab edge, gradually increasing away from this edge.

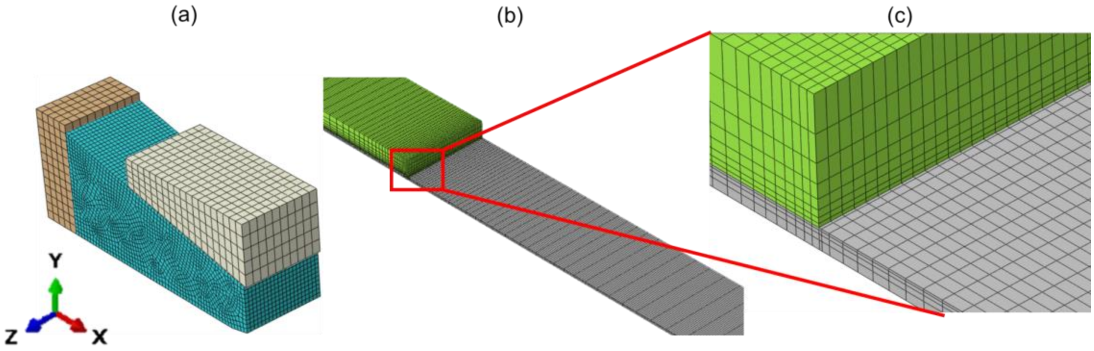

Fig. 3 *Mesh density: a) for the machine components, b) for the specimen, and c) at the edge of the end tabs.*

The tensile test was simulated in two steps with the following boundary conditions:

1. Inward displacement of plunger by 0.75 mm to lock the grip with the specimen and simulate contact pressure. The machine components are fixed after this step as the specimen is considered gripped. To allow for the possible motion of the wedge grip during tensile testing, which could also happen during experiments, the nodes of the wedge grip at the specimen-wedge grip interface were assigned as slave.
2. Applied longitudinal displacement in the central cross-section of the specimen equivalent to 1% strain.

The average longitudinal stress over the cross-section in the center of the specimen is considered as the nominal stress. In all cases, the stress varied less than 3% in this cross-section over the width and thickness of the specimen. The relative overstressing with respect to nominal stress was determined as longitudinal stress concentration factor (SCF). The SCF is calculated by dividing the longitudinal stress at the nodes by the nominal stress. The SCF is computed along the length of the specimen, through a path intersecting the node with maximum stress.

To model the butterfly shape specimen, the effect of longitudinal splitting along with the effect of each fiber end in the curved section should be considered. To model the combination of these effects, the open end of a fiber at the beginning of the curved section is modeled with a cohesive surface (mode II fracture toughness: 1002 J/m^2 and shear strength: 60 MPa [23]) to account for potential splitting (see Fig. 4).

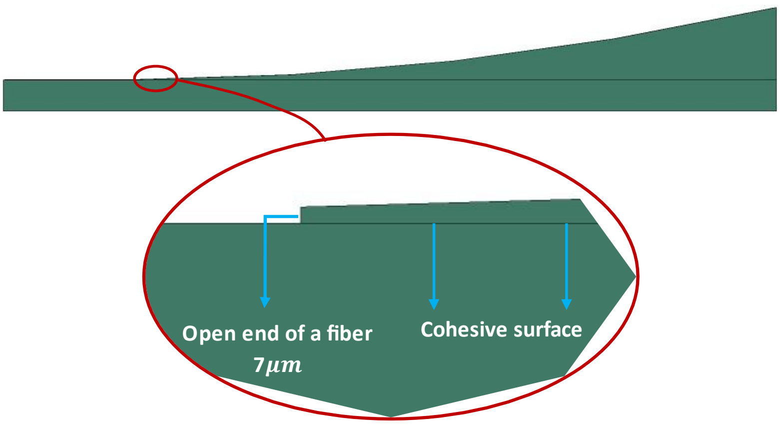

Fig. 4 *Model description of butterfly shape specimen.*

3 Results and discussion

In the following sub-sections, first, the experimental results are discussed. Next, the FE simulation results are utilized to understand the effect of specimen geometry mostly on the longitudinal stress distribution and support the experimental data.

3.1 Experimental study

Fig. 5 presents experimental representative tensile diagrams for different end tabs and specimen geometries. Tests without end tabs yield low failure strain values. In general, reducing the end tab thickness or testing without end tabs reduces the geometric discontinuity and consequently the stress concentrations. However, end tabs should be used and they should be thick enough to avoid damage caused by the serrated surface of the grip [8,24]. The absence of the end tab causes surface damage and hence lowers the strength and failure strain, as confirmed in Fig. 5. The same results were obtained in [25,26]. High-strength materials like UD carbon/epoxy laminates require high grip pressures to hinder the sliding of the specimen during the test. The high grip pressure creates considerable surface damage and hence premature failure. Therefore, it is necessary to use end tabs with the proper thickness (1-2 mm) for tensile testing of UD composites [24].

The ASTM standard test with rectangular end tabs yields significant differences compared to tests without end tabs. However, the multiaxial stress concentration induced by (1) the geometric discontinuity and (2) the constraint on the Poisson contraction caused by clamping pressure at the forward edge of the end tab results in premature failure. The experimental tensile results of tapered end tabs in Fig. 5 reveal that the tapered end tabs slightly increase the tensile strength; however, the p-value of 0.10 indicates the difference is not statistically significant. In addition, the preparation of tapered end tabs and making a consistent tapered angle is not straightforward and requires more effort than rectangular tabs. In addition, the lack of direct gripping pressure on the tapered part may cause delamination of the tab from the UD composite. The growth of delamination may blunt or eliminate the effect of tapering, and the stress concentration at the tip of the delamination crack may cause premature failure.

The failure strain of specimens with continuous tabs is higher than the ASTM standard specimens with rectangular end tab (Fig. 5 and Table 2). Note that the average stress, in this case, is calculated using the full specimen cross-section, and hence does not represent the stress in the carbon layer. The continuous tabs eliminate the stress concentration at the edge of the end tab enabling higher failure strains than the specimen with rectangular end tabs [14]. Recently, Kumar et al. [18] revealed that the rectangular specimen (ASTM specimen) with continuous tabs and without rectangular end tabs may not completely eliminate the stress concentration and ensure the highest failure strain. Furthermore, the hybrid nature of the specimen hampers the direct measurement of stress in the middle carbon plies, and the back-calculation of this stress introduces errors. In case of co-curing the continuous tabs and specimen, there is no control over the thickness of the middle carbon layer. Fig. 6 reveals that it can vary locally by about 40-50% over the width of the specimen, which further hampers the stress back-calculation. It could be a promising method to measure the failure strain of the composite material but not the strength.

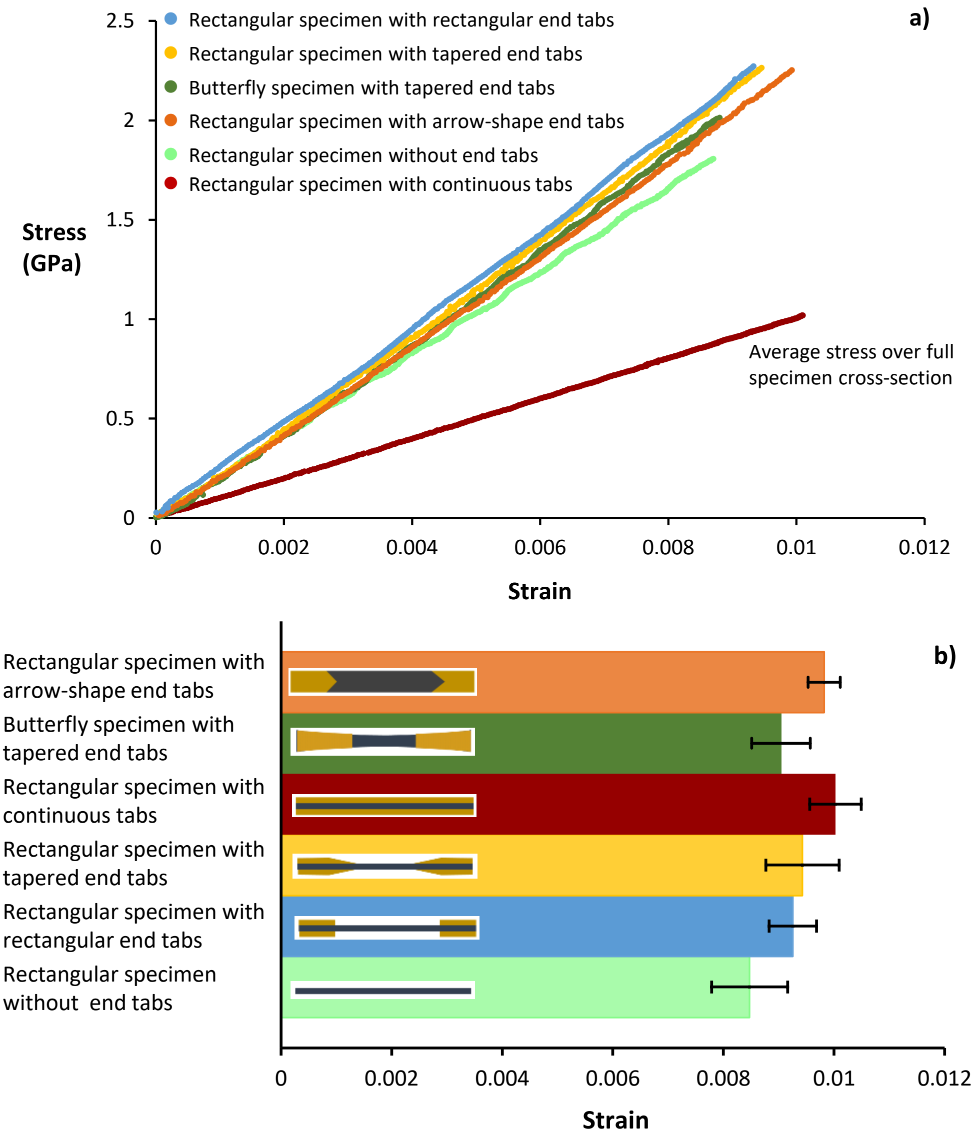

Fig. 5 *Measured failure strains for six different specimen designs: a) representative stress-strain curves and b) average failure strain with error bars showing the standard deviation.*

Fig. 6 *Variation of thickness over the cross-section of the specimen with continuous tabs.*

The butterfly shape specimen is designed to remove the stress concentration from the gauge section of the specimen. However, the results in Fig. 5 indicate lower strength and failure strain compared to the other designs. The main reason is that longitudinal splitting propagates along the specimen length, which counteracts the butterfly shape benefits by reducing the butterfly to a rectangular geometry and causing premature failure. Fig. 7a shows the force-displacement curve of two butterfly shape specimens. The longitudinal splitting initiates at the final stage of failure strain (after 3/4 failure strain) and then propagates upon further load increases. These splits cause unacceptable failure outside of the gauge section (see Fig. 7b). Note that the quality of the cut could affect splitting initiation. Cutting the butterfly specimen requires extra caution to avoid damage to the pristine specimen. The waterjet cutting created a slightly jagged edge that could induce premature splitting (see Fig. 7c). A high-quality cut is vital in the tensile testing of UD composites, and this is easier to achieve with a diamond saw (as done for other specimen designs in this work), and potentially through milling. Note that the milling process of the butterfly specimen, particularly from a thin laminate, is challenging and necessitates expertise and high-quality tools to prevent damage to the edges. However, even this would not avoid splitting [18,27]. Kumar et al. [18] observed longitudinal splitting in milled butterfly specimens made of UD fabric composites.

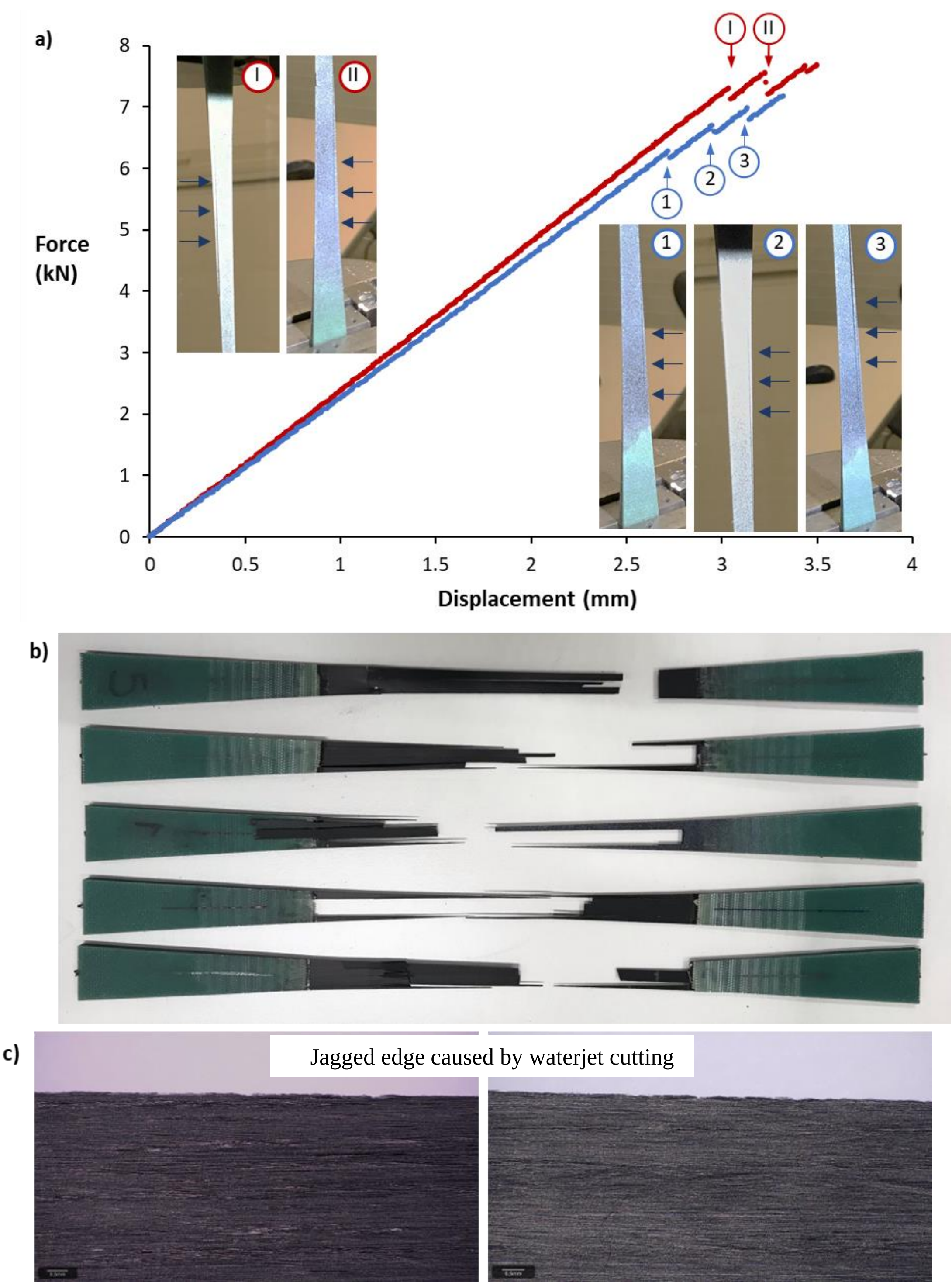

Fig. 7 *Failure in butterfly specimens a) force-displacement curve and longitudinal splitting with arrows indicating the splits, b) specimens after failure, and c) manufacturing defects (from top view).*

The average value of failure strain in the arrow-shape specimen is higher than the standard specimen (rectangular and tapered tabs) (Fig. 5b). Arrow-shape specimens provide moderate stress transition and allow partial Poisson's contraction through the width of the specimen in the tabbed section. The failure strain and strength of the arrow-shape specimen are higher than the rectangular specimen with rectangular end tab and close to the values for the specimen with continuous tabs. The advantages of this design over the continuous tab design are:

1. It does not need any special preparation and can be cut using a band saw or rotating saw. It does not need to be autoclaved. The continuous tab either should be co-cured to the sheet or glued to it before cutting. Note that gluing the continuous tab to the sheet requires expertise to create a good bond all over the sheet to avoid delamination during the test.
2. It provides a uniform cross-section which is not the case in co-cured continuous tab (see Fig. 6),
3. The definition of strength does not need any back-calculation.

Fig. 5b presents the average tensile failure strain of all specimens along with their standard deviation. Table 2 also presents an overview of all experimental data. The strength of the UD carbon layer in the specimen with continuous tab is defined in the following way. First, the tensile test was performed. Then, the specimen was cut from the middle of the upper and lower gripped section (see Fig. 6) and the surfaces of the cut parts were polished. Optical microscopy was used to determine the areal fraction of the carbon and glass layers. The strength is defined using the areal fraction of carbon/glass layers and Table 1 reports their average stiffness. Note that the areal fraction of carbon/glass epoxy was used to define the residual thermal stress in the carbon layer caused by the mismatch in the coefficient of thermal expansion for carbon and glass layers [14]. The strength of the specimen can be defined as:

$$\sigma = f(\varepsilon_{modified}, E) \quad (1)$$

where $\varepsilon_{modified}$ is the strain in the carbon layer after modifying by the thermal coefficient of expansion and E is the carbon layer stiffness. The function f is defined based on the second-order curves that were fitted to the experimental data of rectangular, tapered, and arrow-shape end tab designs.

The highest failure strain is obtained using the arrow-shape specimen and continuous tabs. The analysis (see Table 3) reveals statistically significant differences between arrow-shape and all other designs, as well as between continuous tab and all other designs. The p-value of 0.30 indicates no significant difference between arrow-shape and continuous tab specimens. A p-value smaller than 0.05 was considered statistically significant.

Table 2. Overview of individual and average tensile test results for all designs

Design	Failure strain (%)	Tensile strength (GPa)	Strain (%)		Strength (GPa)		Confidence interval (significance level = 0.05)	
			Average	Standard deviation	Average	Standard deviation	Strain (%)	Strength (GPa)
No end tab	0.93 0.87 0.80 0.78	1.73 1.81 1.95 1.90	0.84	0.069	1.85	0.10	0.067	0.099
Rectangular end tab	0.92 0.89 0.92 0.85	2.40 2.29 2.24 2.10	0.93	0.043	2.33	0.14	0.030	0.099

	0.99	2.21						
	0.95	2.55						
	0.94	2.43						
	0.94	2.38						
	0.89	2.06						
	0.89	1.84						
	0.90	1.93						
	0.98	1.60						
	0.90	2.24						
	0.90	1.86						
Tapered end tab	1.03	2.67	0.94	0.066	2.15	0.32	0.036	0.176
	1.00	2.42						
	1.06	2.53						
	0.91	1.96						
	0.91	2.26						
	1.03	2.42						
	0.86	2.14						
	0.99	2.30						
	1.00	2.32						
	1.05	2.44						
	0.98	2.26						
Continuous end tab	1.05	2.45	1.00	0.047	2.33	0.145	0.029	0.13
	1.07	2.49						
	0.91	2.09						
	0.99	2.30						
	1.00	2.33						
	0.99	2.29						
	0.98	2.006						
	1.02	2.44						
Arrow-shape end tab	0.93	2.05	0.98	0.029	2.23	0.17	0.023	0.137
	0.99	2.25						
	0.99	2.30						
	0.98	2.35						
	0.91	2.0						
	0.88	2.01						
Butterfly shape	0.91	2.02	0.90	0.05	2.07	0.19	0.053	0.22
	0.97	2.41						
	0.85	1.93						

Table 3. p-value of all designs

	Without end tab	Rectangular end tab	Tapered end tab	Continuous tab	Butterfly shape	Arrow-shape
Without end tab	-	0.10	0.059	0.013	0.85	0.023
Rectangular end tab	0.10	-	0.48	0.002	0.43	0.012
Tapered end tab	0.059	0.48	-	0.02	0.19	0.09
Continuous tab	0.013	0.002	0.02	-	0.005	0.30
Butterfly shape	0.21	0.43	0.19	0.005	-	0.016
Arrow-shape	0.023	0.012	0.09	0.30	0.016	-

3.2 Simulation study

The experimental study highlighted the effect of specimen design on the failure strain of the specimen. However, due to the brittle and ‘catastrophic’ failure of UD carbon fiber composites, it is not possible to determine the location where failure starts. The motivation of the simulation study was mainly to understand the longitudinal stress distribution during tensile testing of each specimen design. The simulations were performed with the loading conditions specified in Section 2.3, wherein the plunger is displaced inwards by 0.75 mm to simulate the gripping of the specimen and the specimen center is displaced to achieve a 1% strain.

The maximum stress is observed on the top surface of the specimen (in contact with the end tab/ wedge grip) for all specimen designs. To understand the longitudinal stress distribution for different specimen designs, the SCF is plotted along the distance over the length of the specimen in Fig. 8. To enable better visualization and a direct comparison of SCF in specimens and end tabs of different lengths, the length needs to be normalized. The normalization was done by subtracting the respective end tab length and normalizing it with the gauge length (150 mm) of all presented specimen designs in Fig. 8.

The specimen without end tabs is not included in the comparison. This specimen design is primarily expected to fail due to the serrations in the grip. However, modeling the damage caused by the serrated wedge grip faces is challenging and was not in the scope of the present work. A simulation study with unserrated grip revealed significant stress concentrations in the specimen near the grip end, largely due to limitation in Poisson contraction and the full surface friction condition directly being applied on the specimen-wedge grip interface which is not realistic. The butterfly specimen is excluded from this comparison as the end tabs are outside the gripped section in this design. To understand the cause of failure in butterfly design based on the experimental observations discussed in section 3.1, it was modeled differently than the rest of the specimen types.

Fig. 5 proved that the ASTM standard specimens (rectangular and tapered end tab specimen) exhibited premature failure. The simulation results in Fig. 8 prove that these designs experience longitudinal stress concentrations under the end tabs.

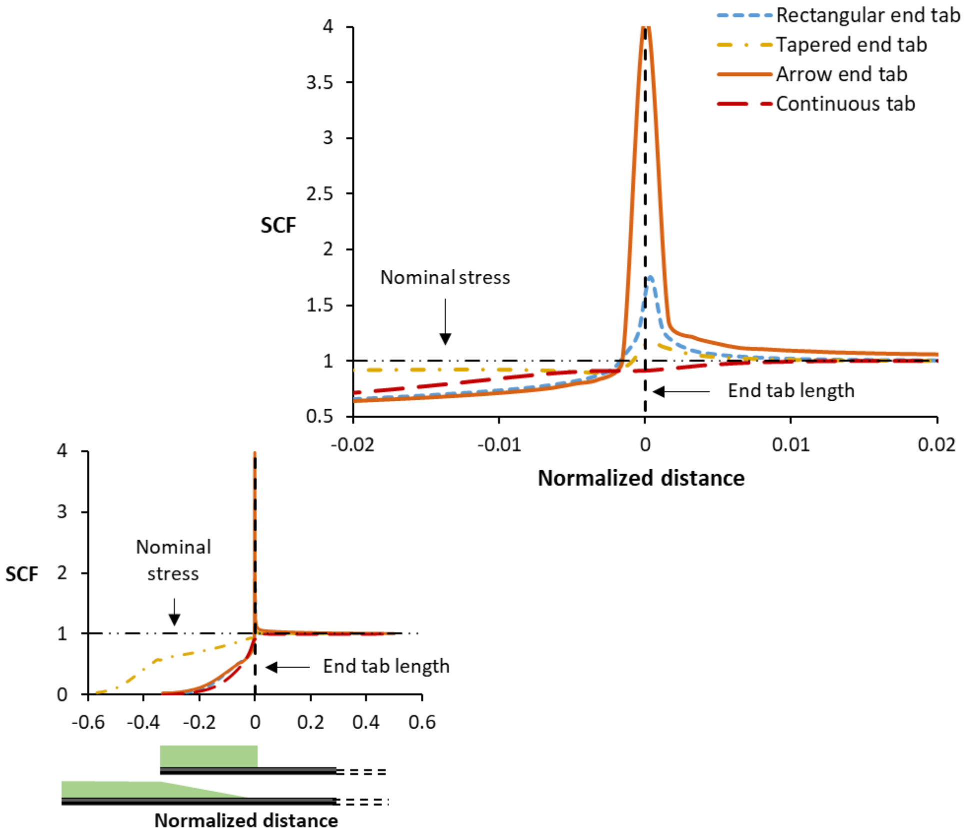

Fig. 8 *Stress distribution under the end tab edge along the length of the specimen*

The high stress concentration at the edge of the rectangular end tab explains the premature failure of the specimen and the likely location for triggering failure. For the tapered end tab specimen, a reduction in stress concentration under the end tab can be seen. However, the stress concentration is not eliminated. Due to the lack of pressure in the tapered region, in addition to longitudinal stress, a complex stress state can develop inside the tapered region, as reported by Levesque et al. [28].

The butterfly shape specimen removed the stress concentration from the gauge section. However, longitudinal splitting can still cause premature failure. This issue comes from the shear stress present in the curved section of the specimen. Fig. 9 proves that the X-butterfly specimen, which is longer than the butterfly specimen reduces the shear stress through the curved section and hence minimizes the effect of longitudinal splitting on the failure strain. Note that the X-butterfly specimen is the same as the butterfly specimen in Fig. 1 except for the length of the end tab being 140 mm instead of 100 mm. Apart from longitudinal splitting, there is also a longitudinal stress concentration at each fiber end in the curved section of the specimen due to the discontinuous geometry. Fig. 10 reveals that the longitudinal stress concentration is not only less significant but also more localized in the X-butterfly specimen than in the butterfly specimen. This is the main reason for the delay of splitting initiation in X-butterfly specimen.

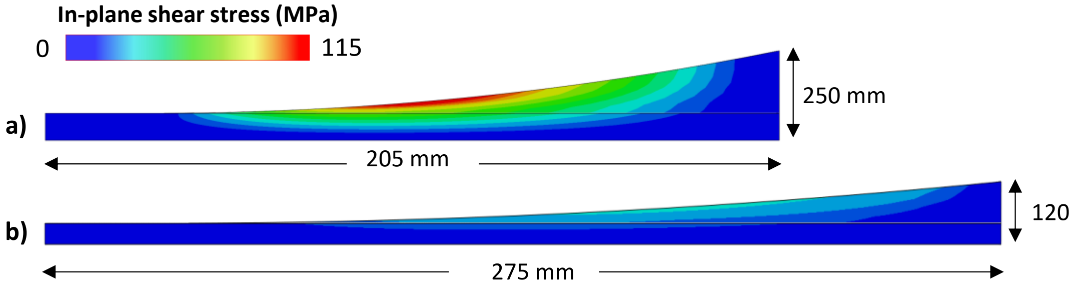

Fig. 9 *Shear stress distribution in a) butterfly and b) X-butterfly specimen.*

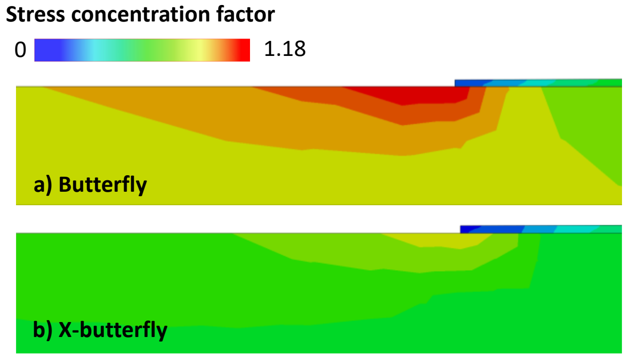

Fig. 10 *Longitudinal stress concentration near the open end of a fiber in the curved section of: a) butterfly and b) X-butterfly specimen.*

The stress distribution for continuous tab specimens indicates that there is no stress concentration in the carbon fiber layer under the end tab edge for the simulated thickness (see Fig. 8), which was the same as the experimentally analyzed one. The stress distribution along the thickness of the specimen reveals that the continuous tab layer acts as a protective cover for the specimen. The high stress concentration due to the change in cross-section at the edge of the end tab is present within the continuous tab and does not reach the carbon fiber layer (see Fig. 11).

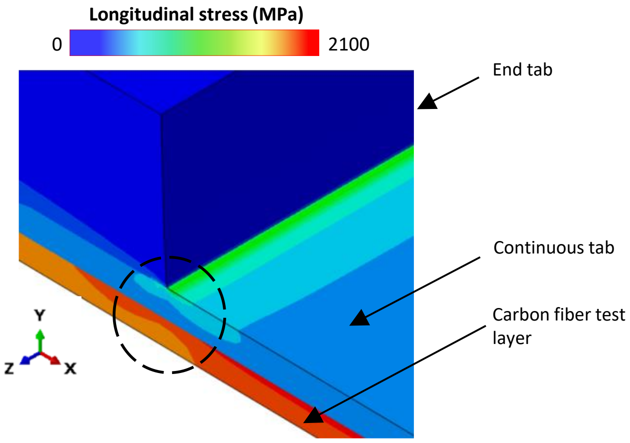

Fig. 11 *Stress distribution in the continuous tab specimen along thickness direction.*

To understand the effect of continuous tab layer thickness on stress distribution, four additional thickness ratios were simulated. To allow a simple demonstration of the effect of thickness ratio (TR), it is defined as the ratio of the total thickness of the carbon fiber layer (t_C) and the thickness of the continuous tab layer (t_{SG}) on each side:

$$TR = t_C / t_{SG} \tag{2}$$

Table 4 summarizes the various thickness ratios that were simulated.

Table 4. Simulated thickness ratios for continuous tab specimen.

Continuous tab thickness each side (mm)	Thickness of carbon fiber test layer (mm)	Thickness ratio
0.28	0.5	1.78
0.42	0.5	1.19
0.56	0.5	0.89
0.70	0.5	0.71
0.84	0.5	0.59

Fig. 12 presents the longitudinal stress distribution for different thickness ratios. Even with the smallest continuous tab thickness, the stress concentration is significantly reduced compared to other specimen designs (see Fig. 8). TR = 1.78 results in the highest stress, but it is only slightly higher than the nominal stress.

As the thickness ratio decreases, the SCF decreases. For TR > 1, stress concentrations are observed, while for TR ≤ 1, stress concentration is negligible. Therefore, thickness ratios lower than 1 indicate lower stress concentrations as they correspond to a higher thickness of the protective continuous tab layer. It can be concluded that TR < 1, which refers to the thickness of the continuous tab on either side of the specimen being larger than the specimen thickness, should consistently provide optimal results for this material combination.

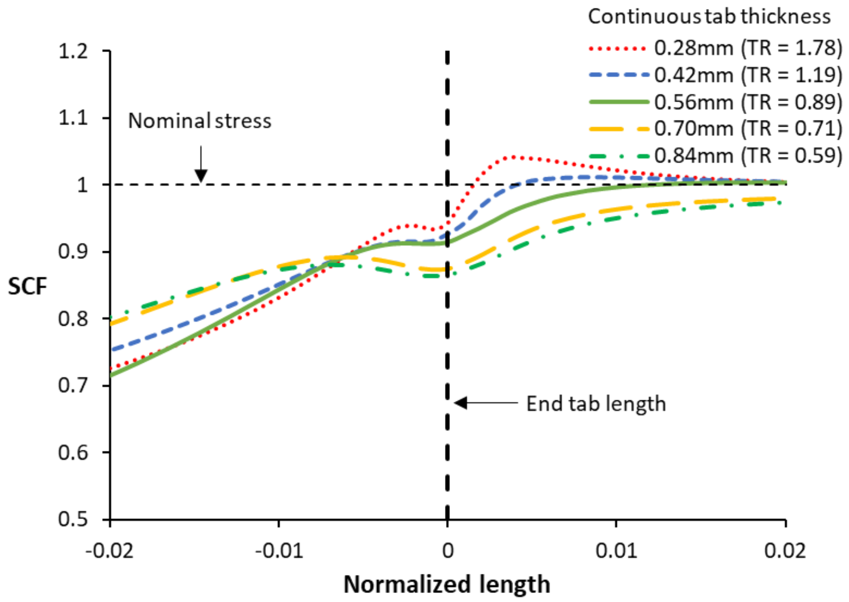

Fig. 12 *Stress distribution along under the continuous tab for different TR configurations.*

Additionally, as noted from the experiments, the strength data needs to be back-calculated in the case of continuous tab specimens due to the hybrid nature of the specimen. As the thickness of the continuous tab increases, the reliability of this back-calculated strength value decreases as the contribution of continuous tab material on the stress back-calculation increases. The failure strain data can be obtained directly and reliably with this design, but the residual thermal strains induced by hybridization must also be considered, especially in the case of co-cured continuous tabbed specimens, as elaborated in Section 3.1 [14]. For this linear elastic simulation study, the thermal strains were not considered. Czel et al. [14] reported that these thermal strains are fairly small for the material combination studied in the present study (less than 5% of total carbon fiber failure strain), and thus their effect on the simulation results is negligible.

The arrow-shape specimen, contradictory to its satisfactory performance in the experiments, displays the highest longitudinal stress concentration under the end tab (Fig. 8). However, the stress concentration is delocalized in the arrow-shape specimen compared to ASTM standard specimens. The arrow-shape specimen was observed to have a 23.5% smaller volume under stresses higher than the nominal stress compared to the rectangular end tab specimen. It can be seen from Fig. 13a that the rectangular end tab has high stress concentrations across the entire width. In the case of arrow-shape end tab, the cross-section along the width in the arrow section is not constant, leading to high stress concentrations only at the geometrical discontinuities along the specimen width, with maximum stress concentration at the arrow tip. Although stress concentrations are significant along the arrow-shape end tab edge (see Fig. 13b), the stress concentration along the width of the specimen is limited to the arrow tip and significantly reduced beyond this point. The volume of material, over which the high stress concentration acts, is much smaller in the arrow-shape end tab than in conventional tab specimens. The stress concentration is also not constant along the edge of the arrow-shape end tab, which leads to further gradual reduction in the specimen volume under high stress concentration. Due to the presence of size scaling of the strength of composites, the SCFs in the arrow-shape specimen would be less detrimental to strength measurements.

This supports the experimental observation of obtaining high failure strain for arrow-shape specimen. Kumar et al. [29] demonstrated the effect of specimen geometry on probabilistic failure according to Weibull's weakest link theory through analytical equations. However, to perform similar quantification for arrow-shape specimen, a numerical analysis needs to be performed which is out of scope for the present study.

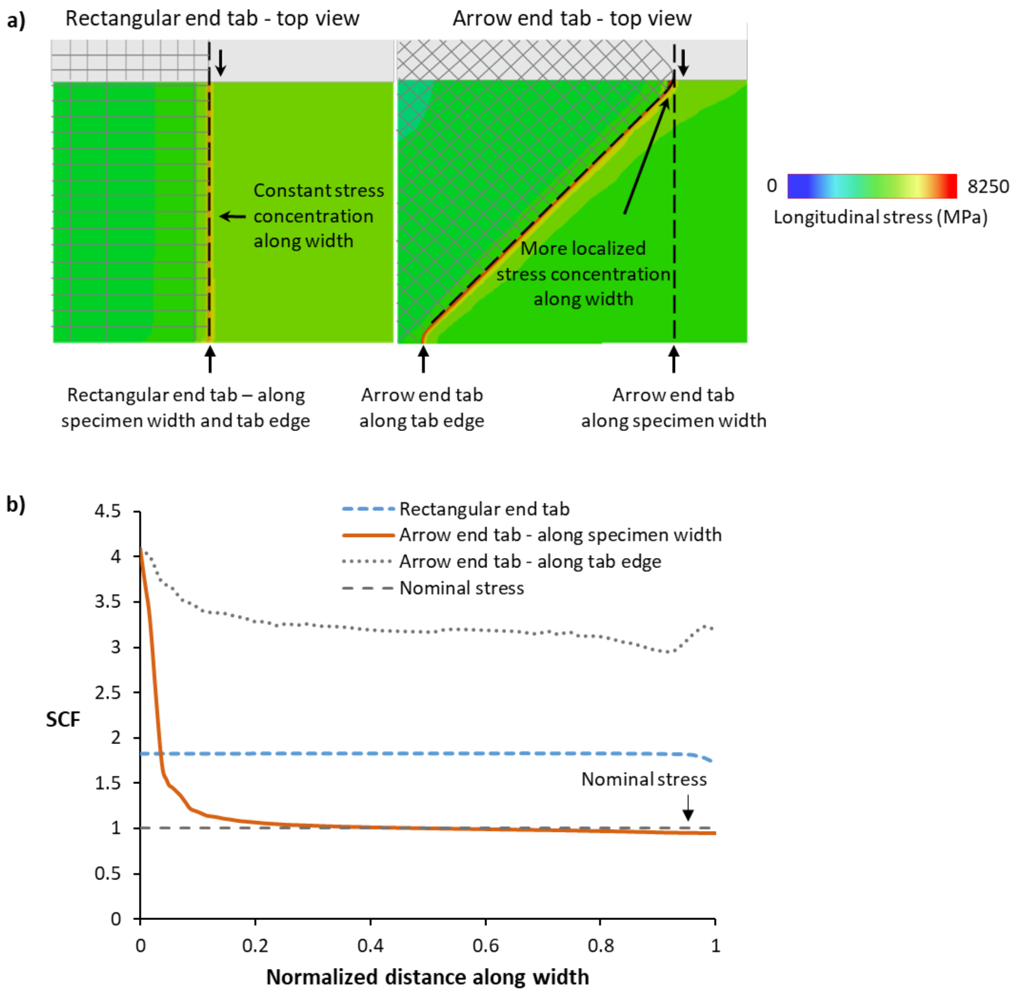

Fig. 13 *a) Longitudinal stress contour for the rectangular end tab and arrow-shape design along the end tab edge in the width direction, and b) stress distribution along the width of the rectangular end tab and arrow-shape design. 0 corresponds to the center of the specimen width, indicated in (a) by black arrows.*

The gradual stress transition due to the arrow-shape is also evident in Fig. 14. The in-plane transverse strain along the marked lines in Fig. 14b and c is plotted along the width of the specimen. The in-plane transverse stress and strain in rectangular specimens originate from the constraint applied by the end tab and the gripping pressure. The transverse strain in the arrow-shape specimen is extracted along three lines (Fig. 14c), passing through the arrow edge (line 1), partially inside and partially outside the end tab (line 2) and completely within the end tab (line 3). For this design, the strain remains fairly constant through the width of the specimen and no significant Poisson's contraction can be seen. The high strain value can be attributed to transverse contraction in the region just at the end tab edge. The variation in the cross-section of the arrow-shape end tab along the width allows partial Poisson contraction (line 1 and line 2). It can be seen from line 2 that the region outside the end tab only experiences a low transverse strain while it spikes at the edge of the end tab. The section of this line that falls completely inside the tabbed region shows very little transverse strain. This is also similar to the region of the specimen where the end tab cross-sectional variation is not present (line 3).

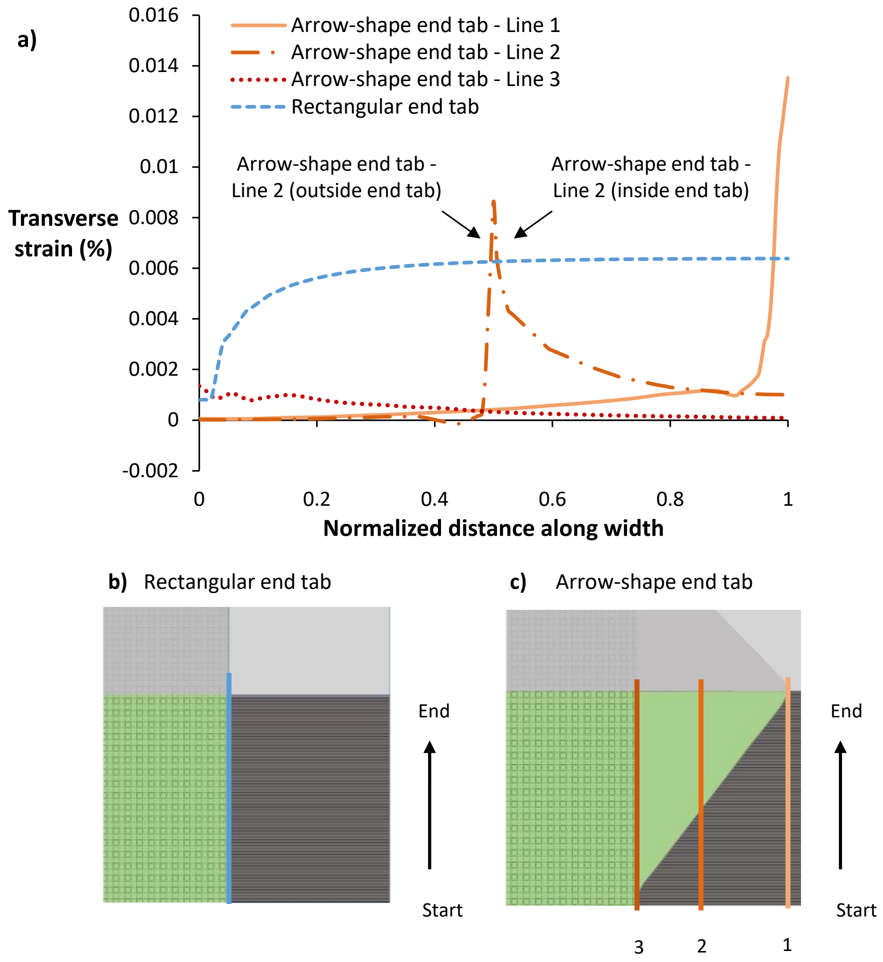

Fig. 14 *a) in-plane transverse strain variation along selected width paths of b) rectangular end tab and, c) arrow-shape end tab specimen.*

The stress distribution points out that arrow-shape specimen can be a potential alternative to conventional end tab specimen. It is easy to implement as it does not require additional material and the tensile test data can be directly utilized for the characterization of failure strain as well as strength.

3.3 Optimization of end tab geometry

The arrow-shape specimen was based on the hypothesis of a more gradual transition over a certain length from the tabbed region to the specimen. This aims to minimize the development of localized stress concentrations in a single cross-section, as presented in the rectangular end tab specimen. While sections 3.1 and 3.2 confirmed this hypothesis, this does not imply that the arrow-shape is the optimal shape to achieve the maximum failure strain. To examine other viable end tab designs based on the same strategy, several other end tab designs were analyzed with the same tab thickness.

Fig. 15 presents the longitudinal stress distribution in specimens with different end tab designs. All the specimens were strained linearly to a 1% remote strain. The geometry of the end tabs can significantly reduce the area under high stress concentrations. The arrow-shape end tab creates a very local hotspot with high stress concentrations. The blunted arrow-shape specimen slightly reduces the stress concentration; however, it is spread over a larger part of the end tab edge with high stress concentration located in one cross-section at the blunt part of the specimen (see Fig. 15b). The circle- and ellipse-shape end tab significantly reduce the longitudinal stress concentration (see Fig. 15 c and d, respectively) as well as transverse (through the thickness) and shear (in-plane) stress components (see Fig. 16). Although the value of stress components in the ellipse-shape end tabs are lower than the circle-shape end tab, the longitudinal stress is more localized over the length close to the forward edge of the ellipse-shape end tab which makes it a critical area for premature failure. Note that this is not a hot spot like the one in arrow-shape end tab but rather a concentration over a certain length at the forward edge of the ellipse-shape end tab. Therefore, specimens with circle-shape end tabs were prepared to experimentally determine the potential improvement. Fig. 17 shows the experimental stress-strain diagrams of 7 specimens with circle-shape end tabs. The measured failure strain of the circle-shape specimen was 1.0% with a standard deviation of 0.03%. The failure strain increases by about 2.6% compared to the arrow-shape specimen, which could not be considered statistically significant.

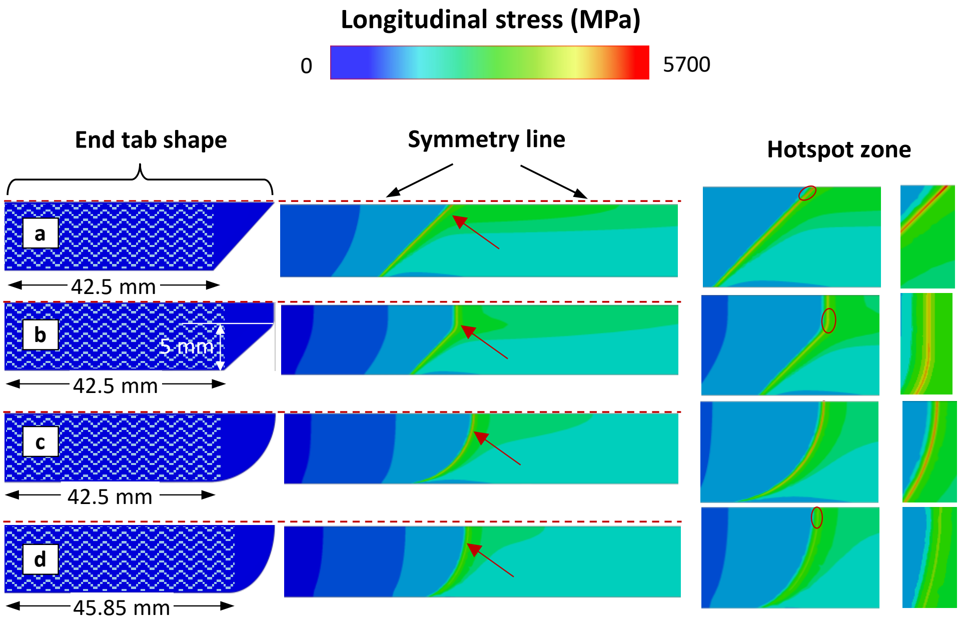

Fig. 15 *Longitudinal stress distribution in different end tabs designs: (a) arrow-shape, (b) blunted arrow-shape, (c) circle-shape, and (d) ellipse-shape. The wavy pattern on the end tabs indicates the grip areas.*

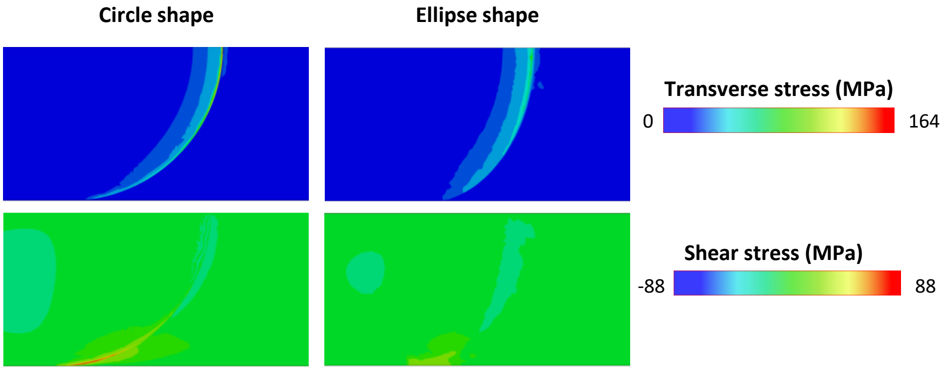

Fig. 16 *Transverse and shear stress distributions in circle- and ellipse-shape end tabs*

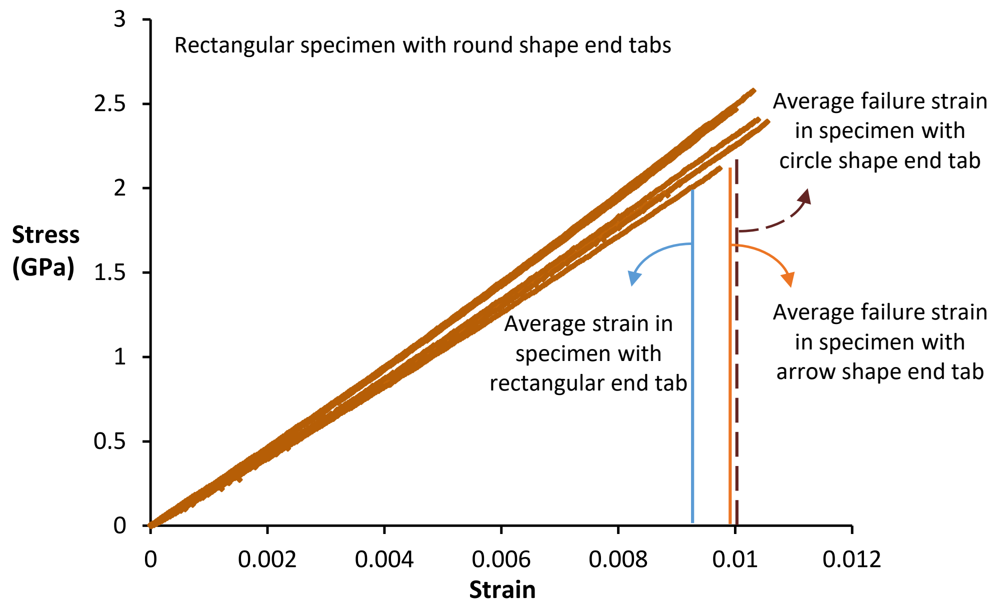

Fig. 17 *Stress-strain curves of specimens with circle-shape end tabs, in comparison with average failure strains for specimens with rectangular and arrow-shaped specimens*

4 Conclusions

Tensile tests were performed on UD carbon/epoxy composites with different designs to determine the best geometry that prevents premature specimen failure. A simulation study was carried out to understand the stress distribution and possible location of failure initiation for each design. Based on this combined experimental-numerical analysis, the following conclusions can be drawn:

1. End tabs are indispensable for performing reliable tensile tests on UD carbon fiber composites.
2. The rectangular and tapered end tab specimens, recommended by the ASTM standard, likely fail prematurely close to the end tab edge because of high stress concentrations near the end tab edge. The tapered end tab alleviates the stress concentration and hence slightly increases the failure strain. However, the lack of clamping pressure over the tapered section may cause delamination, which could result in premature failure.
3. The butterfly specimen failed at a slightly lower strain than other designs, even though the stress is relatively uniform in the gauge section of this design. The main reasons for low failure strain are edge damage due to waterjet cut and premature longitudinal splitting.
4. The continuous tab specimen prevents the stress concentration and hence yields the highest failure strain. The numerical study indicated that a minimum continuous tab thickness can eliminate longitudinal stress concentrations from the specimen. This minimum thickness of the continuous tab layer was found to be equal to the thickness of the carbon fiber layer, for the material combination used in the present study.
5. Calculating the strength in continuous tab specimen is not straightforward and needs back-calculation. In the case of co-curing specimen with continuous tabs, it is even harder because the carbon layer thickness is not consistent.
6. The arrow-shape specimen yielded almost the same failure strain as the continuous tab specimen. The simulations indicate that the stress concentration is highly localized in this specimen design;

therefore, only a small volume of the specimen is under a stress concentration factor equal to 4.08. Due to size scaling, a more localized longitudinal stress concentration should be less detrimental to strength than a lower stress concentration over a larger area. The arrow-shape specimen is a promising approach to measure failure strain and strength and is easier to manufacture than the continuous tab or butterfly specimens.

7. Further optimization of the end tabs geometry confirms we can further lower stress concentrations compared to the arrow-shape design. The circular end tab provides lower stress concentration over a smaller volume than other end tab designs. The circular end tab shows 2.6% improvement in failure strain compared to the arrow-shape; however, the difference is not statistically significant.

While the specimen design directly affects the results of the tensile test, the effects of other parameters, such as test setup (grip alignment, specimen alignment) and manufacturing process (cutting quality, alignment during laminating) are also important and must be studied to further improve the accuracy and reliability of tensile tests.

Acknowledgments

The work leading to this publication was performed within the framework of HyFiSyn project and has received funding from the European Union’s Horizon 2020 research and innovation programme under the Marie Skłodowska-Curie grant agreement No. 765881. The authors would like to acknowledge Professor Sergei B. Sapozhnikov for his helpful discussion and for proposing potential end tab designs.

5 References

[1] De Baere I, Van Paepegem W, Hochard C, Degrieck J. On the tension-tension fatigue behaviour of a carbon reinforced thermoplastic part I: limitations of the ASTM D3039/D3479 standard. Polym Test 2011;30:625–32.

[2] ASTM D3039/D3039M. Standard Test Method for Tensile Properties of Polymer Matrix Composite Materials. ASTM Int West Conshohocken, PA 2000.

[3] ISO 527-1. Plastics - Determination of tensile properties - Part 1: General principles 2019.

[4] Yoo J, Huh H, Lim J, Lee T. Tensile properties of CFRP manufactured by resin transfer molding considering stacking sequences at various strain rates. J Compos Mater 2019;53:2015–30.

[5] Tahir MM, Wang WX, Matsubara T. A novel tab for tensile testing of unidirectional thermoplastic composites. J Thermoplast Compos Mater 2019;32:37–51.

[6] De Baere I, VanPaepegem W, Degrieck J. On the design of end tabs for quasi-static and fatigue testing of fibre-reinforced composites. Polym Compos 2008;30:381–90.

[7] Hojo M, Sawadat Y, Miyairi H. Influence of clamping method on tensile properties of unidirectional CFRP in 0 ° and 90 ° directions- round robin activity for international standardization in Japan 1994;25:786–96.

[8] Kulakov V, Tarnopol’skii Y, Arnautov A, Rytter J. Stress-strain state in the zone of load transfer

in a composite specimen under uniaxial tension. Mech Compos Mater 2004;40:91–100.

[9] Portnov GG, Kulakov VL, Arnautov AK. A refined stress-strain analysis in the load transfer zone of flat specimens of high-strength unidirectional composites in uniaxial tension 2. Finite-element parametric analysis. Mech Compos Mater 2007;43:29–40.

[10] Da Silva LFM, D Adams R. Techniques to reduce the peel stresses in adhesive joints with composites. Int J Adhes Adhes 2007;27:227–35.

[11] Khan B, Potter K, Wisnom MR. Suppression of delamination at ply drops in tapered composites by ply chamfering. J Compos Mater 2006;40:157–74.

[12] Portnov GG, Kulakov VL, Arnautov AK. A refined stress-strain analysis in the load transfer zone of flat specimens of high-strength unidirectional composites in uniaxial tension 3. effect of grip misalignment. Mech Compos Mater 2007;43:495–504.

[13] Portnov GG, Kulakov VL, Arnautov AK. A refined stress-strain analysis in the load transfer zone of flat specimens of high-strength unidirectional composites in uniaxial tension 1. theoretical analysis. Mech Compos Mater 2006;42:547–54.

[14] Czél G, Jalalvand M, Wisnom MR. Hybrid specimens eliminating stress concentrations in tensile and compressive testing of unidirectional composites. Compos Part A Appl Sci Manuf 2016;91:436–47.

[15] Kumagai S, Shindo Y, Horiguchi K, Takeda T. Mechanical characterization of CFRP woven laminates between room temperature and 4 K. JSME Int Journal, Ser A Solid Mech Mater Eng 2003;46:359–64.

[16] Korkiakoski S, Brøndsted P, Sarlin E, Saarela O. Influence of specimen type and reinforcement on measured tension-tension fatigue life of unidirectional GFRP laminates. Int J Fatigue 2016;85:114–29.

[17] De Baere I, Van Paepegem W, Hochard C, Degrieck J. On the tension-tension fatigue behaviour of a carbon reinforced thermoplastic part II: Evaluation of a dumbbell-shaped specimen. Polym Test 2011;30:663–72.

[18] Kumar R, Mikkelsen LP, Lilholt H, Madsen B. Experimental Method for Tensile Testing of Unidirectional Carbon Fibre Composites Using Improved Specimen Type and Data Analysis. Materials 2021;14:393–9.

[19] Mesquita F, Bucknell S, Leray Y, Lomov S V., Swolfs Y. Single carbon and glass fibre properties characterised using large data sets obtained through automated single fibre tensile testing. Compos Part A Appl Sci Manuf 2021;145:106389.

[20] Chamis CC. Mechanics of Composite Materials: Past, Present, and Future. J Compos Technol Res 1989;11:3–14.

[21] Cunningham ME, Schoultz S V, Toth JM. Effect of End-Tab Design on Tension Specimen Stress Concentrations. In: Vinson JR, Taya M, editors. Recent Adv. Compos. United States Japan, West Conshohocken, PA: ASTM International; 1985, p. 253–62.

[22] Engineering Toolbox Friction - Friction Coefficients and Calculator. Https://WwwEngineeringtoolboxCom/Friction-Coefficients-D_778Html n.d.

[23] Turon A, Camanho PP, Costa J, Renart J. Accurate simulation of delamination growth under mixed-mode loading using cohesive elements: Definition of interlaminar strengths and elastic stiffness. Compos Struct 2010;92:1857–64.

[24] Daniel O. Adams; Donald F. Adams. Tabbing guide for composite test specimens. Utah uni salt lake city dep od mechanical engineering; 2002.

[25] Matsuo T, Hojo M, Kageyama K. Influence of gripping method on tensile properties of unidirectional thermoplastic CFRP – Round-robin activity for international standardization in Japan. J Compos Mater 2019;53:4161–71.

[26] Matsuo T, Hojo M, Kageyama K. Influence of gripping condition and matrix type on tensile properties of unidirectional carbon fiber reinforced thermoplastic composites. ICCM Int Conf Compos Mater 2017;2017-Augus:20–5.

[27] Nijssen RPL. Phenomenological fatigue analysis and life modeling. Fatigue life Predict. Compos. Compos. Struct., Woodhead Publishing Series in Composites Science and Engineering; 2010, p. 47–78.

[28] Lévesque M, Gilchrist MD, Fisa B. A theoretical study of the tensile test for highly anisotropic composite materials. ASTM Spec Tech Publ 2003:320–35.

[29] Kumar R, Madsen B, Lilholt H, Mikkelsen LP. Influence of Test Specimen Geometry on Probability of Failure of Composites Based on Weibull Weakest Link Theory. Materials 2022;15:3911.